Technical University of Denmark

DTU

Aerodynamic and load control performance testing of a morphing trailing edge flap system on an outdoor rotating test rig
Paper

Barlas, T K; Olsen, Anders Smærup; Aagaard Madsen , Helge; Løgstrup Andersen, Tom; Ai, Q; Weaver, P M

DTU Library
Technical Information Center of Denmark

PAPER • OPEN ACCESS

Aerodynamic and load control performance testing of a morphing trailing edge flap system on an outdoor rotating test rig

View the article online for updates and enhancements.

Aerodynamic and load control performance testing of a morphing trailing edge flap system on an outdoor rotating test rig

T K Barlas[1], A S Olsen[1], H Aa Madsen[1], T L Andersen[1], Q Ai[2], P M Weaver[2]

[1] Department of Wind Energy, Technical University of Denmark (DTU), DTU Risø Campus, Frederiksborgvej 399, 4000 Roskilde, Denmark.

[2] Advanced Composites Centre for Innovation & Science (ACCIS), University of Bristol, Queen's Building, University Walk, Bristol, BS8 1TR, U. K.

Corresponding author: T K Barlas - tkba@dtu.dk

Abstract. A testing campaign utilizing DTU's outdoor rotating rig is described, where a novel morphing flap system developed in collaboration with the University of Bristol within the INNWIND.eu project has been evaluated and successfully demonstrated. In addition, the aerodynamic performance of ECN's newly designed aerofoil has been evaluated in atmospheric conditions. The morphing wing is shown to achieve good performance in terms of aerodynamic lift control, and compares well with computational fluid dynamics predictions. Moreover, simple feed-forward controller implementations, also utilizing inflow sensors, show promising results in terms of dynamic load alleviation.

1. Introduction

Testing the performance and robustness of innovative smart blade technology has been an important part of the INNWIND.EU project [1]. Wind tunnel testing of present flap systems has been already performed in a variety of campaigns and has verified the actuation concepts and aerodynamic performance in a wind tunnel environment. However, there is big step from wind tunnel testing on a stationary blade section to full scale turbine application and therefore a so-called rotating test rig has been developed at DTU and has been already utilized in testing active flap systems [2] [3]. The main objective is to test the aerodynamic and load control performance of a developed morphing trailing edge flap system on a new aerofoil under realistic inflow conditions on the rotating test rig.

2. Description of the rotating rig and the blade section with the morphing flap

The rotating rig situated at the test field at Risø campus of the Technical University of Denmark (DTU), is based on the former 100 KW Tellus turbine, where the rotor is replaced by an elastic beam and a counterweight and is driven by a motor with a frequency converter in order to control the rotational speed. On the outer part of the 10m beam a 2m span and 1m chord blade section is mounted and instrumented with surface pressure sensors on the mid span position and two five-hole pitot tubes for measuring the local inflow to the blade (Figure 1). Finally, metrological data such as wind speed and wind direction is measured in three heights in a nearby met mast. For testing of the University of Bristol (UoB) morphing flap design, a wind turbine blade profile, ECN-G30-18-60 [4] designed by ECN in the INNWIND.EU project, was realized. The blade mid-section is instrumented with 57

pressure taps distributed in the chord-wise direction. Two of the taps are installed inside the trailing edge of the flap. Furthermore, 16 pressure taps are distributed in the span of the wing at the 27% of the chord length from the leading edge. The eight uniform 20% chord morphing trailing edges developed at the UoB [5], which have a span of 249mm each, are actuated in a connected motion using a linear motion servo-motor (Figure 1). The morphing flap device consists of four components: 1) a carbon fibre reinforced plastic (CFRP) laminate upper skin on the suction side of the aerofoil; 2) a 3D printed honeycomb core of zero Poisson's ratio along the aerofoil chord providing the through-thickness support to the structure; 3) a silicon lower skin on the pressure side to provide a smooth aerodynamic surface and 4) a carbon fibre rod with a diameter of 2 mm as an actuation rod.

Figure 1. Left: The morphing flap mounted on the blade section, Centre: The blade section mounted on the rotating rig boom before installation. Right: The rotating rig with the mounted blade section.

3. Test cases

It is important to observe the performance of the blade section and active flap at a range of angles of attack and Reynolds numbers representative of the scenarios in which the active flap could eventually operate on a MW-scale turbine. The angle of attack range is roughly +/-15 degrees under a normal production scenario. The angle of attack is determined by wind speed, rotor speed, and boom pitch. The Reynolds number is determined by wind speed and rotor speed and should be at least 1 million, and preferably 3 – 10 million. Due to vibration restrictions, the rig can only operate up to roughly 20rpm, while the boom pitch is limited to +15/-15 degrees about zero. Although the flap is capable of a maximum range of ±10deg, the flap angle range in all tests has been limited to ±5deg in order to limit any risk of placing extreme stress on the actuator. In all cases the rotor is placed at the mean wind direction. The test matrix is defined with the target to test the average aerodynamic performance of the morphing wing, its transient response, and its load control capability.

The following cases are tested in this campaign:
- Flap steps: Steps of the flap angle to its maximum angle range around the neutral position for average aerodynamic polars in atmospheric conditions and flap effectiveness.
- Periodic feed-forward flap control: Azimuth-based flap angle variation to counteract periodic loading due to yaw misalignment.
- Inflow feed-forward flap control: Proportional flap command based on filtered Pitot tube inflow angle.

In the flap step cases, 5min tests are conducted with the flap angle fixed at zero, as well as with step changes in flap angle every 10 seconds for a range of pitch settings. This is sufficient to measure both the transient and steady state response of the aerodynamics to the changing flap angles. For the case of square flap input signals, the derived aerodynamic data is averaged over smaller periods during the flap activation cycle. In all cases a square input of 0.025 Hz is used, so the flap activation cycle is

divided into 4 sections of 10s each. The positive flap region is defined as the 1st section, the neutral flap region as the 2nd section, and the negative flap region is defined as the 3rd section. This is shown in Figure 2, where the positive (towards the pressure side), neutral (undeflected) and negative (towards the suction side) flap regions are shown in red, black and green, respectively. A range of steady pitch setting cases are measured, where positive pitch corresponds to nose down ('to feather') direction.

The second type of cases concerns prescribed azimuth-based flap control, which comprise 5min time series with the flap activated once per revolution towards its maximum positive or negative angles in order to counteract 1P periodic loading fluctuations. The flap signal is a 0.33Hz harmonic signal (1/rev) with a tuned phase, which comprises an approximate half-sinusoidal signal from zero flap angle to either maximum positive or negative flap deflection (Figure 2). All cases are conducted at a pitch setpoint of -5 deg., which corresponds, to an average angle of attack close to the design point. The flap is scheduled to be active for two revolutions, followed by two revolutions of no flap activation. In order to test this periodic controller, cases where the rotor is placed at an average of 30deg yaw misalignment are measured. A photo of the flap activation seen from the connection of the wing to the boom during the tests is shown in Figure 3.

The third type of cases concerns inflow-based feed-forward flap control, which comprise 5min with the flap activated with a proportional gain on the band-pass filtered inflow angle from the outboard Pitot tube. The inflow angle signal is filtered between 0.04Hz-1Hz, in order to remove the static gain and react to frequencies up to 3P. The proportional gain is tuned in order to achieve maximum flap angle range for the maximum variation of the inflow. No model-based feed-forward controller design is utilized, so the response is not optimized considering the physical and filter delays.
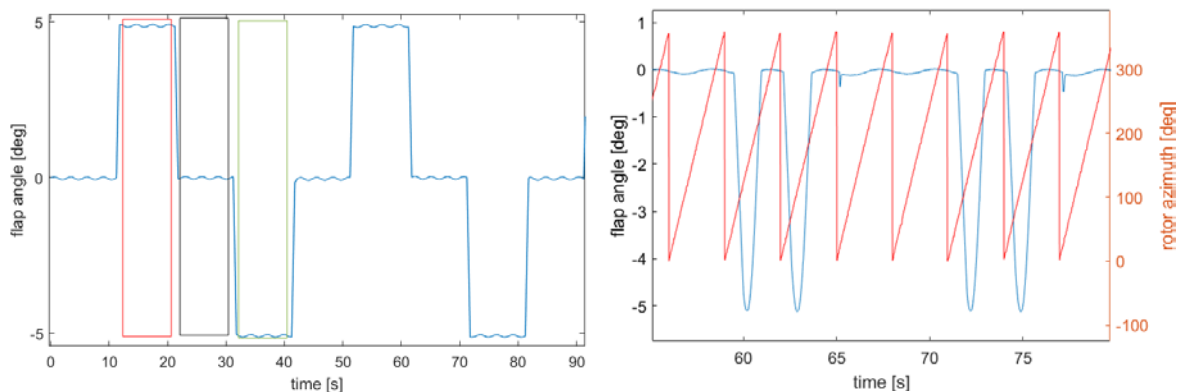

Figure 2. Left: Flap step signal indicating time periods of flap states for data binning. Right: Flap signal as a function of the rotor azimuth (activation at a phase-delayed blade top position in this case).

Figure 3. Photo of wing with deflected flap during operation.

The full test matrix is shown in Table 1.

Table 1. Test cases in the rotating rig experiments.

case	rotor speed [rpm]	pitch angle [deg]	flap	runs	duration [min]
1	20	0	no	2	5
2	20	0	steps	2	5
3	20	5	no	2	5
4	20	5	steps	2	5
5	20	10	no	2	5
6	20	10	steps	2	5
7	20	15	no	2	5
8	20	15	steps	2	5
9	20	-15	no	2	5
10	20	-15	steps	2	5
11	20	-10	no	2	5
12	20	-10	steps	2	5
13	20	-5	no	2	5
14	20	-5	steps	2	5
15	20	-5	azimuth control	8	5
16	20	-5	inflow control	2	5

4. Test results

The integrated aerodynamic forces at the wing section are calculated from the pressure tap measurements on the aerofoil, also utilizing the Pitot tube pressure measurements. In one part of the post-processing the local flow angle and local flow velocity are derived from the Pitot tube pressure differences. In the other part of the post-processing, the chordwise pressure tap data is utilized and corrected in order to derive the integrated aerodynamic forces and coefficients.

For the flap step cases, the pressure data are post-processed and C_L values are sorted based on the angle of attack and flap angle average values. It is seen that the uncorrected binned measured polars have an angle of attack offset and reduced slope compared to EllipSys 2D CFD [6] fully turbulent RANS (Figure 4). This is due to 3D induction effects, upwash on the Pitot tube measurement point

and an identified pressure drop in the measurement system (which only results in an offset of the angle of attack). Corrections are utilized in order to establish an accurate translation of aerodynamic measurements on the rotating rig to 2D aerodynamic polars. The pressure drop discrepancy is corrected by comparing the pressure distributions to the CFD data, the Pitot tube upwash effect is derived based on simple 2D vorticity upwash, and the 3D induction effects are derived from Hawc2 simulations using the near-wake model [7][8]. The corrected data then is shown to compare well with 2D CFD, especially in the linear region (Figure 4). The binned corrected data for all average flap positions are then shown and compared to EllipSys 2D CFD fully turbulent RANS data in Figure 5. It is seen that the overall aerodynamic impact of the flap is captured well, with average estimated variations in the linear region of $\Delta C_L = +0.2$ and $\Delta C_L = -0.25$ for the $+5^o$ and -5° flap angle respectively. The CFD data provide estimated average variations of $\Delta C_L = +0.25$ and $\Delta C_L = -0.3$.
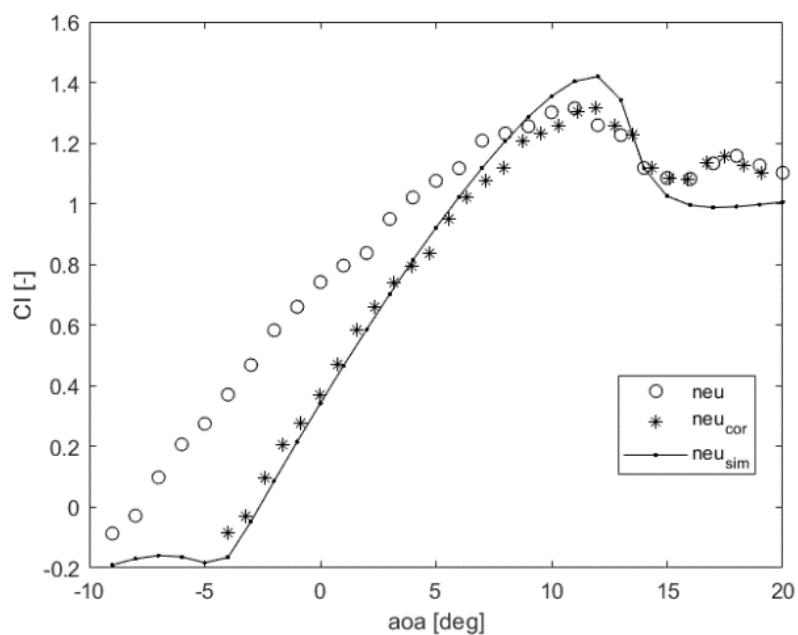

Figure 4. Binned measured C_L data for samples without flap (*neu*). Data corrected for 3D effects and Pitot tube pressure offset (*neu_{cor}*). Comparison with 2D CFD data (*neu_{sim}*)
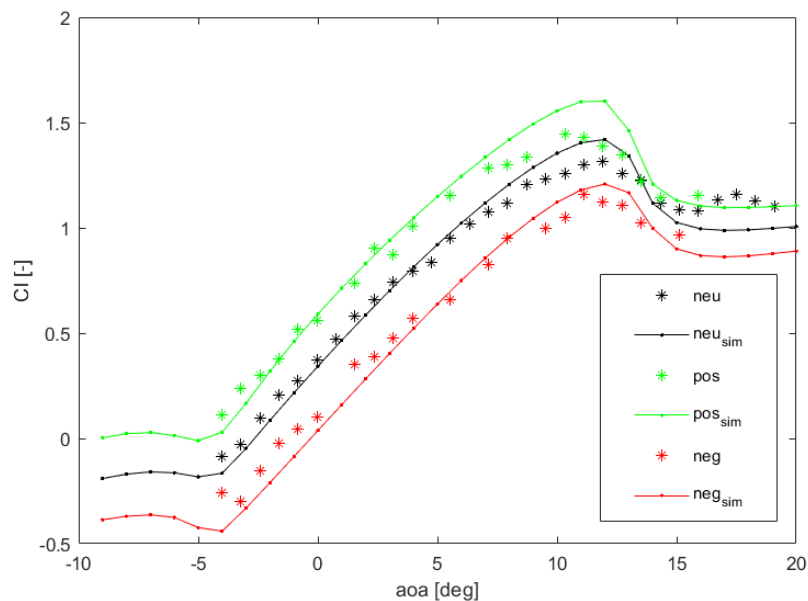
Figure 5. Binned measured C_L data for samples without flap (*neu*), +5º flap (*pos*) and -5 º flap (*neg*) as a function of inflow angle. Comparison with 2D CFD data (*neu$_{sim}$*, *pos$_{sim}$*, *neg$_{sim}$*).

The pressure coefficient data (Cp) are also binned around the design angle of attack of 8º for the baseline and flap angle range samples. The binned data are shown and compared to EllipSys 2D CFD data in Figure 6. It is seen that the overall Cp curve shape is captured well, along with the effect of the flap deflections. Considering that the measured curve is an average representation of the measured data, main differences appear at the leading edge region, which can be attributed to surface roughness and inflow turbulence effects.
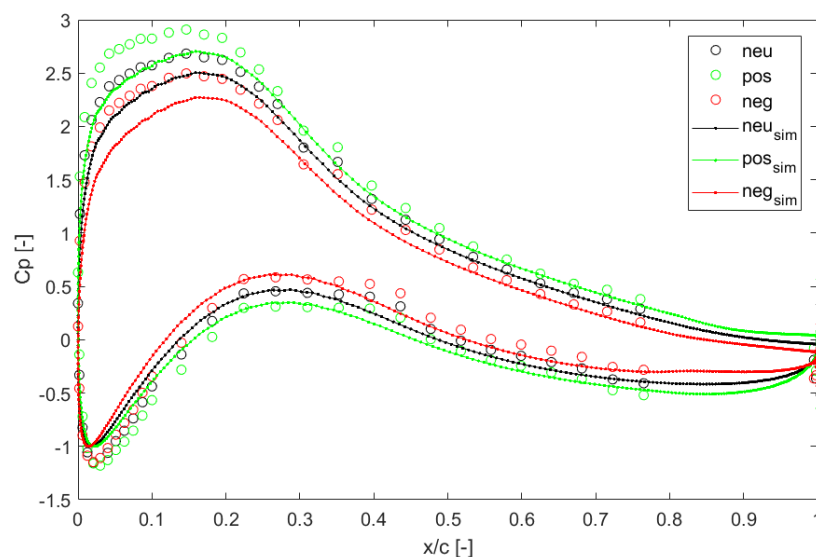

Figure 6. Binned measured Cp data at 8 º inflow angle for samples without flap (*neu*), +5 º flap (*pos*) and -5 º flap (*neg*) as a function of inflow angle. Comparison with 2D CFD data (*neu$_{sim}$*, *pos$_{sim}$*, *neg$_{sim}$*).

The prescribed azimuth-based flap control comprise 5min time series with the flap activated once per revolution towards its maximum positive or negative angles in order to counteract 1P periodic loading

fluctuations. The flap signal is a 0.33Hz harmonic signal (1/rev) with a tuned phase, which comprises an approximate half-sinusoidal signal from zero flap angle to either maximum positive or negative flap deflection (Figure 7). All cases are conducted at a pitch setpoint of -5 deg., which corresponds, to an average angle of attack close to the design point. The flap is scheduled to be active for two revolutions, followed by two revolutions of no flap activation. In order to test this periodic controller, cases where the rotor is placed at an average of 30deg yaw misalignment are measured. The data from the flapwise strain sensor is post-processed and sorted for every sample consisting of two revolutions without control and two revolutions with the flap controller active. The statistics of every consecutive samples are then compared. The time series of the flapwise moment at the connection of the wing to the boom is shown in Figure 7, together with the flap angle which is activated for two revolutions followed by two revolutions without activation. The flap angle is driven to the maximum negative angle of -5deg when the blade is at its top position, targeting the alleviation of peak loading. The comparison of the standard deviation of the flapwise moment for every consecutive sample of no activation and azimuth-based flap activation is shown in Figure 7. Although, as expected, the prescribed azimuth-based flap activation is not robust, it results in an average reduction of the standard deviation of the flapwise moment of 12%.
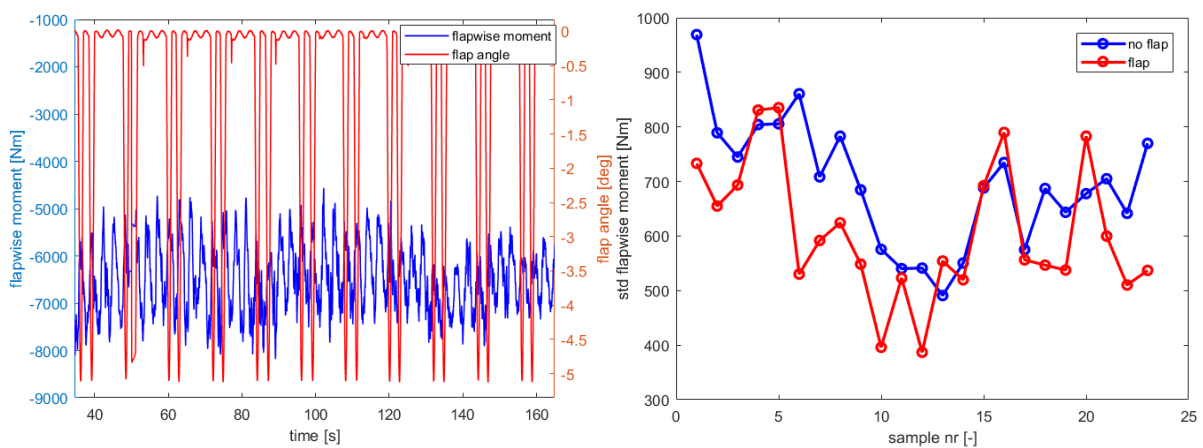

Figure 7. Left: Time series of flapwise moment and azimuth-based flap activation. Right: Comparison of standard deviation of flapwise moment with azimuth-based flap activation.

For the inflow flap control cases, the data from the flapwise strain sensor are post-processed and sorted for every sample consisting of 10s without control and 10s with the feed-forward inflow-based flap controller active. The statistics of every consecutive samples are then compared. The time series of the flapwise moment at the connection of the wing to the boom are shown in Figure 8, together with the flap angle which is activated for 10s followed by 10s without activation. The flap angle in this case reacts to fluctuations of the inflow angle within the band-pass filtered range of frequencies up to 3P. The comparison of the standard deviation of the flapwise moment for every consecutive sample of no activation and inflow-based flap activation is shown in Figure 8. The flap controller results in an average reduction of the standard deviation of the flapwise moment of 11%.
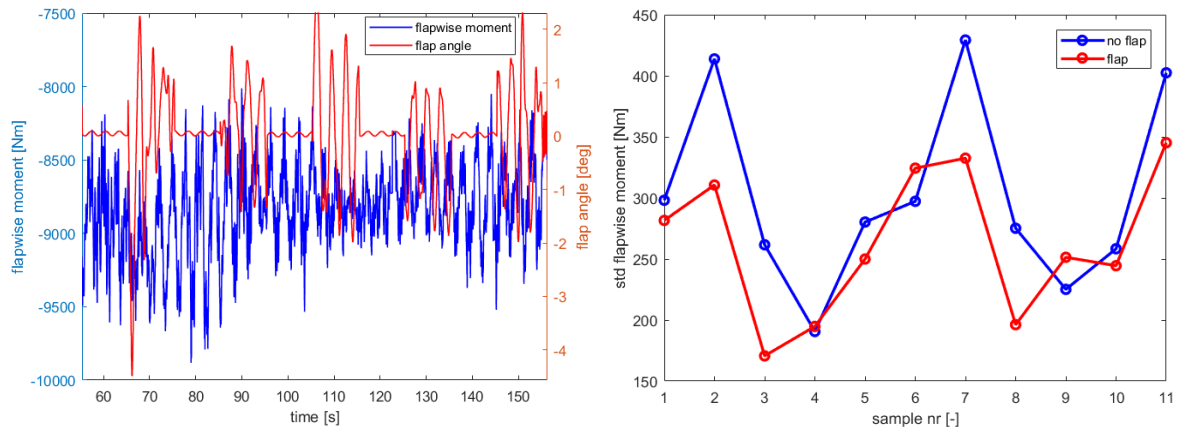
Figure 8. Left: Time series of flapwise moment and inflow-based flap activation. Right: Comparison of standard deviation of flapwise moment with inflow-based flap activation.

5. Conclusions

In the testing campaign utilizing DTU's rotating rig, the morphing flap technology developed in collaboration with the University of Bristol has been evaluated and successfully demonstrated. It is shown that the morphing wing achieves good performance in terms of aerodynamic load response, close to numerical estimations. Moreover, simple controller implementations show promising results in terms of dynamic load alleviation. In addition, the aerodynamic performance of ECN's new aerofoil has been evaluated in atmospheric conditions. Future work should focus on evaluating the performance of advanced controllers in a similar setup.

References

[1]   INNWIND.EU - Innovative Wind Conversion Systems (10-20MW) for Offshore Applications, www.innwind.eu.
[2]   Madsen, HA, Barlas, A & Løgstrup Andersen, T 2015, A morphing trailing edge flap system for wind turbine blades, Proceedings of the 7th ECCOMAS Thematic Conference on Smart Structures and Materials (SMART 2015).
[3]   Barlas, A & Aagaard Madsen, H 2015, Atmospheric Full Scale Testing of a Morphing Trailing Edge Flap System for Wind Turbine Blades. in Proceedings. 26th International Conference on Adaptive Structures and Technologies.
[4]   Madsen, HA et al., New airfoils for high rotational speed wind turbines, INNWIND.EU Deliverable 2.12.
[5]   Ai, Q, Weaver, PM, & Azarpeyvand, M 2017, Design and mechanical testing of a variable stiffness morphing trailing edge flap. Journal of Intelligent Material Systems and Structures, DOI: 10.1177/1045389X17721028.
[6]   Sørensen, NN, 2015, General purpose flow solver applied to flow over hills, Technical Report Risø-R-827(EN).
[7]   Larsen, TJ & Hansen, AM 2007, How 2 HAWC2, the user's manual. Risø National Laboratory. Denmark. Forskningscenter Risoe. Risoe-R, no. 1597(ver. 3-1)(EN).
[8]   Pirrung, G, Hansen, MH & Aagaard Madsen , H 2014, 'Improvement of a near wake model for trailing vorticity' Journal of Physics: Conference Series (Online), vol 555, 012083. DOI: 10.1088/1742-6596/555/1/012083.